# Modeling of THz Chip-to-Chip Wireless Channels in Metal Enclosures

Alenka Zajic and Prateek Juyal Georgia Institute of Technology, Atlanta, GA 30332 USA

Abstract—In this paper, we consider chip-to-chip communication such as processor to memory link where the motherboard is placed in a casing similar to a desktop or a laptop. At THz frequencies, the dimensions of the casing are large enough that signal may reflect from the objects inside the box and the sides of the box creating resonant cavity effect. To model propagation in such an environment, we model casing as overmoded cavity and consider other objects in the casing as conductive objects. We propose a geometry-based statistical propagation model that describes chip-to-chip propagation in metal enclosures filled with conductive objects. Based on the geometrical model, a simulation model for multipath fading in this cavity is developed and correlation function is derived. The simulation results show that multiple reflections created in the resonant cavity significantly impact correlation function and power delay profile and need careful consideration when modeling chip-to-chip propagation in metal enclosures.

### I. INTRODUCTION

Data communication between computer components, such as processor and memory within a computer system, currently relies on metal wires [1]- [3]. The future demand for pins that connect processor and memory as the number of cores in the processor increases will make packaging challenging because the number of pins that a small chip package can have is limited, Additionally, sophisticated connections can make component insertion (e.g. during assembly) and removal (e.g. to replace a failed component) more time-consuming and costly [4]- [6].

Wireless communication can alleviate such serviceability and packaging constraints [7]- [11]. Integration of wireless transceivers and antennas into the chip package would provide communication bandwidth without adding pins to the chip package. A key challenge for wireless communication is that the required data rates in existing systems are already in the hundreds of gigabits per second. For example, within a server computer system, data rates already exceed 500 Gbits/s, e.g. since late 2014 the Intel Core i7 Extreme processors [12] and most Intel Xeon E5 v3 processors [13] can communicate with the systems main memory using four DDR4-2133 channels, with a total throughput of 533 Gbits/s, and this is expected to soon increase to 800 Gbits/s when DRR4-3200 support is introduced.

Achieving such per-link data rates is unlikely to be feasible for wireless communication at mm-Wave frequencies. As an

This work has been supported, in part, by NSF grant 1651273. The views and findings in this paper are those of the authors and do not necessarily reflect the views of NSF.

example, WiGig [14] uses 60 GHz frequency range to provide up to 7 Gbits/s using OFDM, 64-QAM, and sophisticated coding, and 4.7 Gbits/s WiGig devices are already available [15]. Even with 7 Gbits/s per channel, more than 75 such channels need to be combined to match the existing processor-memory data rates (533 Gb/s). With each antenna several millimeters in size, such a 75-channel link is unlikely to be feasible for integration into a chip package that is typically less than 3 centimeters on each side. On the other hand, terahertz (THz) wireless communication has two key advantages that can be combined to achieve the required data rates. First, the usable frequency band around each frequency is much larger, so each channel can have a much higher data rate. Second, the antenna size at THz frequencies allows for large number of antennas packed in a small operating space.

To enable chip-to-chip THz wireless communications, it is imperative to understand propagation mechanisms that govern communication in the unique propagation environment of a computer system (motherboard) at these high frequencies and to develop models to characterize such an environment. First measurements efforts to characterize THz chip-to-chip environment have been reported in [16]- [19], and first modelling efforts to characterize reflections from printed circuit board surfaces have been reported in [20].

In this paper, we consider chip-to-chip communication such as processor to memory link where the motherboard is placed in a casing similar to a desktop or a laptop. At THz frequencies, the dimensions of the casing are large enough that signal may reflect from the objects inside the box and the sides of the box creating resonant cavity effect. To model propagation in such an environment, we model casing as overmoded cavity and consider other objects in the casing as conductive objects. We propose a geometry-based statistical propagation model that describes chip-to-chip propagation in metal enclosures filled with conductive objects. Based on the geometrical model, a simulation model for multipath fading in this cavity is developed and correlation function is derived. The simulation results show that multiple reflections created in the resonant cavity significantly impact correlation function and power delay profile and need careful consideration when modeling chip-to-chip propagation in metal enclosures.

The remainder of the paper is organized as follows. Section II introduces the geometry-based statistical model and presents a parametric model for the overmoded cavity loaded with conductive objects. Section III describes over-moded cavity characterization and derives space-time correlation func-

tion. Section V provides concluding remarks.

# II. GEOMETRY-BASED STATISTICAL MODEL FOR CHIP-TO-CHIP COMMUNICATIONS IN METAL ENCLOSURES

This section considers propagation between a stationary transmitter  $(T_{\rm x})$  and a single stationary receiver  $(R_{\rm x})$  placed in an over-moded cavity loaded with conductive objects. An example of such a scenario is processor-to-memory link on a computer motherboard inside a desktop casing. For this analysis, both the  $T_{\rm x}$  and  $R_{\rm x}$  probes are assumed to be omnidirectional, positioned on the motherboard and surrounded with other metal objects on a motherboard.

A metal enclosure can be considered an overmoded cavity when it permits the excitation of a large number of modes with closely proximate resonant frequencies. Typically, overmoded cavity operates at frequencies that have very high mode density (i.e. the number of modes that can be excited per given bandwidth of frequencies should be large). This is typically satisfied at THz frequencies for computer enclosures. Hence, it is important to take into account overmoded cavity propagation effect.

The field distribution of the excited modes creates locations of high and low field magnitudes called hot and cold spots, respectively. This can be a problem for antenna positioning because some of the locations in the cavity are more preferable than others. However, if the conductive objects are present in the cavity, the hot and cold spots are perturbed which changes the spatial power distribution inside the cavity. This can increases the probability of signal reaching all locations in the cavity.

To model the impact of conductive objects in the cavity, we assume three propagation mechanisms: 1) some waves from the T<sub>x</sub> antenna may traverse directly to the R<sub>x</sub> antenna (LoS rays), 2) others are single-bounced at the  $T_x$  (i.e., the waves from the  $T_x$  antenna scatter from the scatterers located around the T<sub>x</sub> before arriving at the R<sub>x</sub> antenna), single-bounced at the  $R_{\rm x}$  (i.e., the waves from the  $T_{\rm x}$  antenna scatter from the scatterers located around the Rx before arriving at the  $R_x$  antenna), and 3) some waves that are mode generated in the cavity, before they arrive at the Rx, impinge on one of the conductive objects around the Tx and at one of the conductive objects around the  $R_{\rm x}$  before arriving at the  $R_{\rm x}$ antenna. These propagation mechanisms are illustrated in Fig. 1. The model assumes that we have scatterers  $S_t^{(m,n,p)}$  and  $S_r^{(m,n,p)}$ , uniformly distributed on circles around the  $T_x$  and R<sub>x</sub>, respectively. For the model presented here, theoretically the scatterers should be positioned on spheres around the  $T_x$ and R<sub>x</sub>, but due to practical constraints regarding positions of the  $T_x$  and  $R_x$  and loading objects (it is unlikely that they will be hanging in the air), we assume only a two-dimensional distribution of scatterers.

In the model, it is assumed that  $N_t$  and  $N_r$  fixed omnidirectional scatterers are uniformly distributed around the circles with radii  $\Delta R$  around the  $T_x$  and  $R_x$ , respectively . The distance between the  $T_x$  and  $R_x$  is D. The number of scatterers  $N_t$  and  $N_r$  depends on the number of modes generated in the

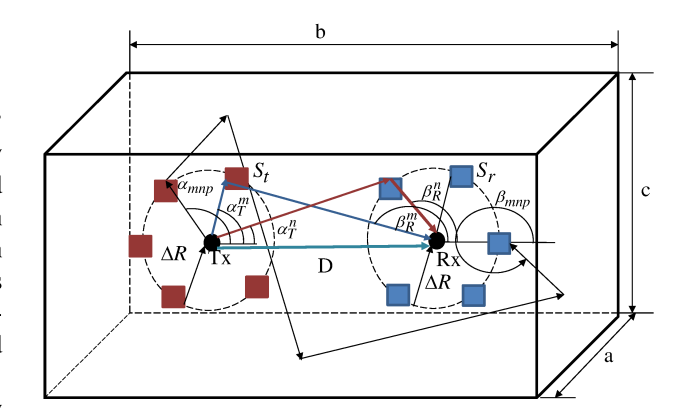


Fig. 1. The geometry-based statistical model of chip-to-chip communications in metal enclosures loaded with scatterers.

overmoded cavity, because each of the modes will be perturbed by the scatterer in the vicinity of the receiver. The number of modes in a rectangular cavity is a function of frequency and can be calculated as [21]

$$N_s(f) \approx \frac{8\pi f^3 V}{3c_0^3},\tag{1}$$

where f is the frequency of excitation,  $V = a \cdot b \cdot d$  is the volume of the rectangular cavity, and  $c_0$  is the speed of light in a vacuum.

The radii  $\Delta R$  of the circles represent the additional excess path traveled by each mode in the overmoded cavity. This excess path can be related to frequency deviation required to change the excited mode distribution as follows:

$$\Delta R = \frac{c_0}{2\Delta f_m},\tag{2}$$

where frequency deviation  $\Delta f$  can be calculated from [22]

$$\Delta f_m \approx \frac{c_0^3}{8\pi V f^2}.$$
(3)

The symbols  $\alpha_T^m$  and  $\alpha_T^n$  are the angles of departures (AoD) of the waves that impinge on the scatterers  $S_t$  and  $S_r$ , whereas  $\alpha_R^m$  and  $\alpha_R^n$  are the azimuth angles of arrivals (AoA) of the waves scattered from  $S_t$  and  $S_r$ , respectively. Finally, the symbols  $\alpha_{m,n,p}$  and  $\beta_{m,n,p}$  denote the angles of departure (AoD) and the angles of arrival (AoA) of the waves that impinge on scatterers  $S_t$  and scatter from the scatterers  $S_r$  before arriving at the receiver.

Based on the propagation mechanisms assumed in the model, the input delay-spread function of the  $T_x\text{-}R_x$  link can be written as a superposition of the LoS, single-bounced transmit, single-bounced receive and overmoded-multi-bounced rays

$$h(\tau) = h^{SBT}(\tau) + h^{SBR}(\tau) + h^{MB}(\tau) + h^{LoS}(\tau)$$
.(4)

The single-bounced components of the input delay-spread

function are, respectively,

$$h^{SBT}(\tau) = \sqrt{\frac{\eta_T}{K+1}} \frac{1}{\sqrt{N_t}} \sum_{m=1}^{N_t} \xi_m e^{j\phi_m} \delta(\tau - \tau_m), (5)$$

$$h^{SBR}(\tau) = \sqrt{\frac{\eta_R}{K+1}} \frac{1}{\sqrt{N_r}} \sum_{n=1}^{N_r} \xi_n e^{j\phi_n} \delta(\tau - \tau_n),$$
 (6)

where  $\xi_m,\ \xi_n,\ \tau_m,$  and  $\tau_n$  denote the amplitudes and time delays of the multipath components, respectively. The amplitudes of the multipath components,  $\xi_m$  and  $\xi_n$ , are defined

$$\xi_{m} = \frac{\sqrt{P_{t}}\lambda}{4\pi} \left[ \left| d\left(T_{x}, S_{t}^{(m)}\right) \right| + \left| d\left(S_{t}^{(m)}, R_{x}\right) \right| \right]^{-\gamma/2}$$

$$\approx \Omega \left( 1 - \frac{\gamma}{2} \frac{\Delta R}{D} \right), \tag{7}$$

$$\xi_{n} = \frac{\sqrt{P_{t}}\lambda}{4\pi} \left[ \left| d\left(T_{x}, S_{r}^{(n)}\right) \right| + \left| d\left(S_{r}^{(n)}, R_{x}\right) \right| \right]^{-\gamma/2}$$

respectively, where  $P_t$  is the transmit power, K is the Rice factor (ratio of LoS to scatter received power),  $\gamma$  is the path loss exponent,  $d(\cdot, \cdot)$  denotes distance between two points, and  $\Omega = D^{-\gamma/2} \sqrt{P_t} \lambda/4\pi$ . Finally, the time delays  $\tau_m$  and  $\tau_n$  are defined as the travel times of the waves scattered from the scatterers  $S_t$  and  $S_r$ , i.e.,

$$\tau_m = \frac{D + \Delta R(1 - \cos \alpha_T^m)}{c_0} \tag{9}$$

$$\tau_m = \frac{D + \Delta R (1 - \cos \alpha_T^m)}{c_0}$$

$$\tau_n = \frac{D + \Delta R (1 + \cos \alpha_R^n)}{c_0},$$
(9)

where  $c_0$  is the speed of light.

 $\approx \Omega \left(1 - \frac{\gamma}{2} \frac{\Delta R}{D}\right),$ 

The overmoded-multi-bounced component of the input delay-spread function is

$$h^{MB}(\tau) = \sqrt{\frac{\eta_{MB}}{K+1}} \frac{1}{\sqrt{N_t \cdot N_r}}$$

$$\sum_{m=1}^{M} \sum_{n=1}^{N} \sum_{p=1}^{P} \xi_{m,n,p} e^{j\phi_{m,n,p}} \delta(\tau - \tau_{m,n,p}),$$
(11)

where  $\xi_{m,n,p}$  and  $\tau_{m,n,p}$  are the amplitude and time delay of the overmoded-multibounced component, respectively. The amplitude of the overmoded multipath component,  $\xi_{m,n,p}$ , is defined as [23]

$$\xi_{m,n,p} = \frac{E_0}{8} \sum_{i=1}^{8} (-1)^{i+1} \frac{e^{-jkR_{i,m,n,p}}}{R_{i,m,n,p}}.$$
 (12)

The amplitude of the electric field  $E_0$  can be obtained in terms of cavity parameters, i.e.,

$$E_0 = \sqrt{\frac{QP_t}{\omega\epsilon_0 V}}, \tag{13}$$

where  $P_t$  is the power transmitted into the cavity,  $Q \approx f/\Delta f_m$ is the quality factor, V is the volume of the cavity,  $\omega$  is the angular frequency of the transmitted signal, and  $\epsilon_0$  is the permittivity of free space. The distance  $R_{i,m,n,p}$  can be calculated from cavity geometry and positions of the Tx and

$$R_{i,m,n,p} = \sqrt{(x_i^2 + 2ma)^2 + (y_i^2 + 2nb)^2 + (z_i^2 + 2pd)^2},$$
 (14)

where spatial coordinates  $x_i$ ,  $y_i$ , and  $z_i$  are obtained as follows:

$$x_i = \begin{cases} x_T - x_R, & i = 1, 2, 3, 8 \\ x_T + x_R, & i = 4, 5, 6, 7 \end{cases},$$
(15)

$$y_i = \begin{cases} y_T - y_R, & i = 1, 2, 5, 6 \\ y_T + y_R, & i = 3, 4, 7, 8 \end{cases} , \tag{16}$$

$$z_{i} = \begin{cases} z_{T} - z_{R}, & i = 1, 3, 5, 7 \\ z_{T} + z_{R}, & i = 2, 4, 6, 8 \end{cases} , \tag{17}$$

and vectors  $(x_T, y_T, z_T)$  and  $(x_R, y_R, z_R)$  denote the coordinates of the T<sub>x</sub> and the R<sub>x</sub>, respectively. Finally, the time delay  $\tau_{m,n,p}$  is defined as the travel time of the wave impinged on the scatterer  $S_t$ , bounced several times around the box, and scattered from the scatterer  $S_r$ , i.e.,

$$\tau_{m,l,n,k} = \frac{\Delta R}{c_0} \cos(\alpha_{m,n,p}) + \frac{\Delta R}{c_0} \cos(\beta_{m,n,p}).$$
 (18)

The parameters  $\eta_T$ ,  $\eta_R$ , and  $\eta_{MB}$  in (5), (6), and (11), respectively, specify how much the single- and multiple-bounced rays contribute in the total power  $P_t$ , i.e., these parameters satisfy  $\eta_T + \eta_R + \eta_{MB} = 1$ . It is assumed that the angles of departures  $(\alpha_T^m, \alpha_T^n, \alpha_{m,n,p})$  and the angles of arrivals  $(\beta_R^n, \alpha_T^n, \alpha_{m,n,p})$  $\beta_R^m$ ,  $\beta_{m,n,p}$ ) are random variables. Finally, it is assumed that the phases  $\phi_m$ ,  $\phi_n$ , and  $\phi_{m,n,p}$  are random variables uniformly distributed on the interval  $[-\pi,\pi)$  and independent from the angles of departure and the angles of arrival.

The LoS component of the input delay-spread function is

$$h^{LoS}(\tau) = \sqrt{\frac{K}{K+1}} \xi_{LoS} \delta(\tau - \tau_{LoS}), \qquad (19)$$

where the LoS amplitude is  $\xi_{LoS} \approx \Omega$  and the LoS time delay is  $\tau_{LoS} = D/c_0$ .

To simplify further analysis, we will use the transfer function instead of the input delay-spread function. The transfer function is the Fourier transform of the input delay-spread function [24] and can be written as

$$\begin{split} T(f) &= \mathcal{F}_{\tau}\left\{h(\tau)\right\} = \\ &T^{SBT}(f) + T^{SBR}(f) + T^{MB}(f) + T^{LoS}(f), \end{aligned} \tag{20}$$

where  $T^{SBT}(f)$  is the single-bounced transmit,  $T^{SBR}(f)$  is the single-bounced receive,  $T^{MB}(f)$  is the double-bounced, and  $T^{LoS}(f)$  is the LoS component of the transfer function and can be written, respectively, as

$$T^{SBT}(f) = \sqrt{\frac{\eta_T}{K+1}} \frac{1}{\sqrt{N_t}} \sum_{m=1}^{N_t} \xi_m e^{j\phi_m - j2\pi f \tau_m}, (21)$$

$$T^{SBR}(f) = \sqrt{\frac{\eta_R}{K+1}} \frac{1}{\sqrt{N_r}} \sum_{n=1}^{N_r} \xi_n e^{j\phi_n - j2\pi f \tau_n}, (22)$$

$$T^{MB}(f) = \sqrt{\frac{\eta_{MB}}{K+1}} \frac{1}{\sqrt{N_t \cdot N_r}}$$

$$\sum_{m=1}^{M} \sum_{n=1}^{N} \sum_{p=1}^{P} \xi_{m,n,p} e^{j\phi_{m,n,p} - j2\pi f \tau_{m,n,p}}, (23)$$

$$T^{LoS}(f) = \sqrt{\frac{K}{K+1}} \xi_{LoS} e^{-j2\pi f \tau_{LoS}}. (24)$$

## III. CORRELATION FUNCTION OF WIRELESS CHANNEL FOR CHIP-TO-CHIP COMMUNICATIONS IN METAL **ENCLOSURES**

The normalized correlation function (CF) between two transfer functions defined in (20), i.e., T(f) and  $T(f + \Delta f)$ , is defined as

$$R(\Delta f) = \frac{\mathrm{E}\left[T(f)^*T(f+\Delta f)\right]}{\sqrt{\mathrm{Var}[T(f)]\mathrm{Var}[T(f)]}},$$
 (25)

where  $(\cdot)^*$  denotes complex conjugate operation,  $E[\cdot]$  is the statistical expectation operator, and  $\mathrm{Var}[\;\cdot\;]$  is the statistical variance operator. Since  $T^{SBT}(f)$ ,  $T^{SBR}(f)$ , and  $T^{MB}(f)$ are independent complex Gaussian random processes with zero means, (25) can be simplified to

$$R(\Delta f) = R^{SBT}(\Delta f) + R^{SBR}(\Delta f) + R^{MB}(\Delta f) + R^{LoS}(\Delta f), \qquad (26)$$

where  $R^{SBT}(\Delta f)$ ,  $R^{SBR}(\Delta f)$ ,  $R^{MB}(\Delta f)$ , and  $R^{LoS}(\Delta f)$ denote the normalized CFs of the single-bounced transmit, single-bounced receive, double-bounced, and LoS components, respectively, and are defined as

$$R^{SBT}(\Delta f) = \frac{\mathbb{E}\left[T^{SBT}(f)^*T^{SBT}(f + \Delta f)\right]}{\Omega/(1+K)}, \quad (27)$$

$$R^{SBR}(\Delta f) = \frac{\mathbb{E}\left[T^{SBR}(f)^*T^{SBR}(f + \Delta f)\right]}{\Omega/(1+K)}, \quad (28)$$

$$R^{MB}(\Delta f) = \frac{\mathbb{E}\left[T^{MB}(f)^*T^{MB}(f + \Delta f)\right]}{\Omega/(1+K)}, \quad (29)$$

$$R^{LoS}(\Delta f) = \frac{\mathbb{E}\left[T^{LoS}(f)^*T^{LoS}(f + \Delta f)\right]}{\Omega/(K+1)}. \quad (30)$$

$$R^{SBR}(\Delta f) = \frac{\mathrm{E}\left[T^{SBR}(f)^*T^{SBR}(f+\Delta f)\right]}{\Omega/(1+K)}, (28)$$

$$R^{MB}(\Delta f) = \frac{\mathrm{E}\left[T^{MB}(f)^*T^{MB}(f+\Delta f)\right]}{\Omega/(1+K)}, \quad (29)$$

$$R^{LoS}(\Delta f) = \frac{\mathrm{E}\left[T^{LoS}(f)^*T^{LoS}(f+\Delta f)\right]}{\Omega/(K+1)}.$$
 (30)

Substituting (21) into (27) and (22) into (28), respectively, and averaging over angles of arrival and departure, the CFs of SBT and SBR components can be obtained as

$$R^{SBT}(\Delta f) = \eta_T \left( 1 - \gamma \frac{\Delta R}{D} \right) e^{-j\frac{2\pi}{c_0}\Delta f(D + \Delta R)}$$

$$J_0(2\pi \Delta f \Delta R/c_0) \qquad (31)$$

$$R^{SBR}(\Delta f) = \eta_R \left( 1 - \gamma \frac{\Delta R}{D} \right) e^{-j\frac{2\pi}{c_0}\Delta f(D + \Delta R)}$$

$$J_0(-2\pi \Delta f \Delta R/c_0), \qquad (32)$$

where  $J_0(\cdot)$  is the zeroth-order Bessel function of the first kind.

Substituting (23) into (29), and averaging over angles of departure and arrival, the CF function of overmoded-multibounced rays can be written as

$$R^{MB}(\Delta f) = \eta_{MB} \frac{1}{N_t \cdot N_r} \left( \sum_{m,n,p} |\xi_{m,n,p}|^2 \right)$$

$$J_0^2(2\pi \Delta f \Delta R/c_0), \tag{33}$$

where  $J_0(\cdot)$  is the zeroth-order Bessel function of the first kind. The derivations of these expressions are omitted for brevity.

#### IV. SIMULATION RESULTS

In this section, we analyze simulation results for power delay profile (PDP) and correlation function. Since any change in the volume of the cavity will change the excited mode distribution, a set of simulations examining the effect of placing random scattering objects inside the cavity is performed.

The inside dimensions of a cavity are a = 21 cm, = 33 cm, and d = 1 cm, at 300 GHz. The cavity dimensions correspond to typical dimensions of a laptop. The transmit power is assumed to be 1 W to simplify calculations. The transmitter antenna is placed at  $(x_T, y_T, z_T) =$  $(a/2, b/3, 0.001 \,\mathrm{cm})$ , while a receiver antenna is placed at  $(x_R, y_R, z_R) = (a/2, 2b/3, 0.001 \,\mathrm{cm})$ . These locations correspond to middle of the casing. Using Eq. 1, the number of modes is calculated to be  $N_s = 5,805,663$ , and the frequency deviation is found to be  $\Delta f \approx \pm 17.22\,$  kHz. These results verify that this is indeed overmoded cavity.

In simulations, the total number of modes  $N_s$  is approximately equally distributed over all three coordinates, i.e., m = 180, n = 180, and p = 180. The number of scatterers around the transmitter and the receiver are  $N_t = 180^3/2$ and  $N_r = 180^3/2$ , respectively. In all simulations we assume that Ricean factor is K = 1 and that single-bounced and multi-bounced rays contribute equal amount of energy, i.e.  $\eta_T = \eta_R = \eta_{MB} = 1/3.$ 

Figure 2 shows the power delay profile of chip-to-chip channel in metal enclosure. First we can observe that the line of sight component arrives first attenuated by approximately 65 dB. This attenuation corresponds to Friis formula in freespace and is an expected loss. Furthermore, we can observe that multipath components take a long time to reduce its contributions to overall power. This is an expected effect of multiple reflections in the metal enclosure.

Figure 3 plots the correlation functions of single-bounced, multi-bounced, and combined single- and multi-bounced rays. The results show that single-reflected rays stay correlated the longest while multi-reflected rays de-correlate faster. We can also observe that signals get de-correlated after about 10 kHz, which is close to the frequency deviation in the overmoded cavity. This is not surprising result because two modes travel significantly different paths and tend to be uncorrelated. The frequency is somewhat lower than deviation frequency because of the single-bounced rays present in the enclosure.

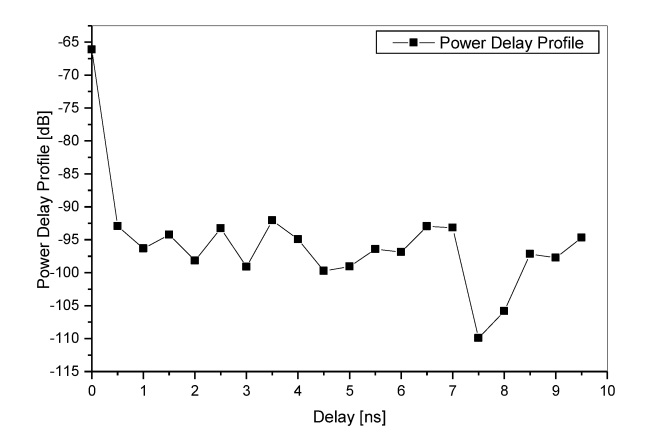


Fig. 2. The power delay profile of chip-to-chip channel in a metal enclosure.

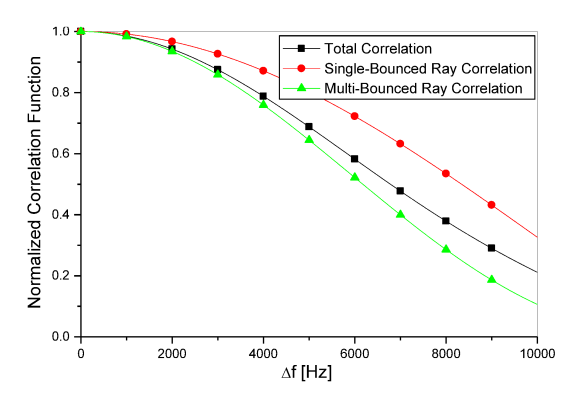


Fig. 3. The correlation functions of chip-to-chip channel in a metal enclosure.

### V. Conclusions

In this paper we considered chip-to-chip communication such as processor to memory link where the motherboard was placed in a casing similar to a desktop or a laptop. Due to electrically large dimensions of the casing at THz frequencies, signal may reflect from the objects inside the box and the sides of the box creating resonant cavity effect. To model propagation in such an environment, the casing was modeled as overmoded cavity and other objects in the casing were considered as conductive objects. A geometry-based statistical propagation model that describes chip-to-chip propagation in metal enclosures filled with conductive objects was proposed. Based on the geometrical model, a simulation model for multipath fading in this cavity was developed and correlation function was derived. The simulation results showed that multiple reflections created in the resonant cavity significantly impact correlation function and power delay profile and need careful consideration when modeling chip-to-chip propagation in metal enclosures.

#### REFERENCES

[1] G. Chen, H. Chen, M. Haurylau, N. Nelson, D. Albonesi, P. Fauchet, and E. Friedman, "On-chip copper-based vs. optical interconnects: delay uncertainty, latency, power, and bandwidth density comparative predictions." *Proc. International Interconnect Technology Conference (IITC)*, 2006.

- [2] N. Srivastava and K. Banerjee, "Performance analysis of carbon nanotube interconnects for VLSI applications," Proc. IEEE/ACM International Conference on Computer Aided Design (ICCAD), 2005.
- [3] A. Naeemi, R. Sarvari, and J. Meindl, "On-chip interconnect networks at the end of the roadmap: limits and nanotechnology opportunities," *International Interconnect Technology Conference (IITC)*, 2006.
- [4] K. Banerjee, S. J. Souri, P. Kapur, and K. C. Saraswat, "3-D ICs: A novel chip design for improving deep-submicrometer interconnect performance and systems-on-chip integration," *Proc. IEEE*, vol. 89, pp. 602-633, May 2001.
- [5] D. A. B. Miller, "Rationale and challenges for optical interconnects to electronic chip," *Proc. IEEE*, vol. 88, pp. 728-749, June 2000.
- [6] R. H. Havemann and J. A. Hutchby, "High-performance interconnects: An integration overview," *Proc. IEEE*, vol. 89, pp. 586-601, May 2001.
- [7] B. A. Floyd, C.-M. Hung, and K. K. O, "Intra-chip wireless interconnect for clock distribution implemented with integrated antenna, receiver, and transmitters," *IEEE J. Solid-State Circuits*, vol. 37, pp. 543-552, May 2002.
- Z. M. Chen and Y. P. Zhang, "Inter-chip wireless communication channel: measurement, characterization, and modeling," *IEEE Transactions on Antennas and Propagation*, vol. 55, pp. 978-986, March 2007.
   D. W. Matolak, S. Kaya, A. Kodi "Channel modeling for wireless networks-on-chips," *IEEE Communications Magazine*, vol. 51, no. 6, pp. 180–186, June 2013.
- [9] J. Gelabert, D. J. Edwards and C. J. Stevens, "Experimental evaluation of UWB wireless communication within PC case," *Electronics Letters*, vol. 47, pp. 773–775, June 2011.
- [10] A. Valdes-Garcia, S. Reynolds, A. Natarajan, and D. Kam, "Singleelement and phased-array transceiver chipsets for 60-GHz Gb/s communications," *IEEE Communications Magazine*, vol. 49, pp. 120–131, April 2011.
- [11] H. Vardhan, N. Thomas, S.-R. Ryu, B. Banerjee, and R. Parkash, "Wireless data center with millimeter wave network," *IEEE Proceeding of GLOBECOM10*, pp. 1–6, December 2010.
- [12] Intel, "Intel Core i7-5960X Processor Extreme Edition", http://ark.intel.com/products/82930
- [13] Intel, "Intel Xeon Processor E5-2697 v3", http:  $//ark.intel.com/products/81059/Intel-Xeon-Processor-E5-2697-v3-35M-Cache-2_60-GHz$
- [14] Wikipedia, Wireless Gigabit Alliance, https //en.wikipedia.org/wiki/Wireless<sub>G</sub>igabit<sub>A</sub>lliance
- [15] Intel, "Intel Tri-Band Wireless-AC 17265 Product Brief,"

  http://www.intel.com/content/www/us/en/wirelessproducts/tri-band-wireless-ac17265-brief.html?wapkw =
  17265
- [16] A. Fricke, S. Rey, M. Achir, P. Le Bars, T. Kleine-Ostmann, and T. Kurner, "Reection and transmission properties of plastic materials at THz frequencies", 38th International Conference on Infrared, Millimeter, and Terahertz Waves (IRMMW-THz), Mainz, Germany, 2013.
- [17] A. Fricke, M. Achir, P. Le Bars, and T. Kurner, "Characterization of transmission scenarios for Terahertz intra-device communications", IEEE-APS Topical Conference on Antennas and Propagation in wireless Communications (APWC), Torino, Italy, 2015.
- [18] S. Kim and A. Zajic, "300 GHz path loss measurements on a computer motherboard," *Proceedings of the 10th European Conference on Antennas and Propagation (EuCAP)*, Davos, Switzerland, 2016.
- [19] S. Kim and A. Zajic, "Characterization of 300-GHz wireless channel on a computer motherboard," *IEEE Transactions on Antennas and Propagation*, vol. 64, no. 12, pp. 5411–5423, Dec. 2016.
- [20] A. Fricke, M. Achir, P. Le Bars, and T. Kurner, "A Model for the reection of Terahertz signals from printed circuit board surfaces", 11th European Conference on Antennas and Propagation (EuCAP), Paris, France, 2017.
- [21] D. A. Hill, Electromagnetic Fields in Cavities. Hoboken, NJ, USA:Wiley, 2009.
- [22] D. A. Hill, Motivation for statistical approaches, in Electromagnetic Fields in Cavities. Hoboken, NJ, USA:Wiley, 2009.
- [23] M. A. K. Hamed and W. A. Johnson, "Ray-optical solution for the dyadic green's function in a rectangular cavity," *IEEE Electronic Letters*, vol. 6, no. 10, pp. 317–319, May 1970.
- [24] A. Zajić, Mobile-to-Mobile Wireless Channels. Norwood, MA, USA: Artech House, Inc., 2013.